Dynamical transition in the temporal relaxation of stochastic processes under resetting

Satya N. Majumdar,[1] Sanjib Sabhapandit,[2] and Grégory Schehr[1]
[1]*Univ. Paris-Sud, CNRS, LPTMS, UMR 8626, Orsay F-01405, France*
[2]*Raman Research Institute, Bangalore 560080, India*
(Received 26 February 2015; published 18 May 2015)

A stochastic process, when subject to resetting to its initial condition at a constant rate, generically reaches a nonequilibrium steady state. We study analytically how the steady state is approached in time and find an unusual relaxation mechanism in these systems. We show that as time progresses an inner core region around the resetting point reaches the steady state, while the region outside the core is still transient. The boundaries of the core region grow with time as power laws at late times with new exponents. Alternatively, at a fixed spatial point, the system undergoes a dynamical transition from the transient to the steady state at a characteristic space-dependent timescale $t^*(x)$. We calculate analytically in several examples the large deviation function associated with this spatiotemporal fluctuation and show that, generically, it has a second-order discontinuity at a pair of critical points characterizing the edges of the inner core. These singularities act as separatrices between typical and atypical trajectories. Our results are verified in the numerical simulations of several models, such as simple diffusion and fluctuating one-dimensional interfaces.

DOI: 10.1103/PhysRevE.91.052131 PACS number(s): 05.40.−a, 02.50.−r, 05.10.Gg

I. INTRODUCTION

Consider a stochastic process evolving under some given dynamics that does not lead to a time-independent stationary state. The prototypical example is the position of a diffusive particle, which has a Gaussian distribution with its width growing as the square root of the time, inferring the absence of a steady state. Now, imagine that by another mechanism, the dynamics is repeatedly being interrupted and recommenced at random times from the initial condition. A general interesting question is: how does such a stochastic resetting affect the temporal evolution of the system?

Examples of stochastic resetting are found in a wide variety of situations. For example, while looking for a friend in a crowded tourist place, after an unsuccessful search over some time period one often returns to the favorite hangout and restarts the search process. In the ecological context, animal movements are often modeled by stochastic processes [1,2]. The movements of foraging animals usually involve a local diffusive search for food, interrupted by long-range nonlocal resetting moves to relocate to other areas as well as to return to their nests, followed by restarting the search process [3]. For instance, the mobility data of free-ranging capuchin monkeys is described quite well by a model of random walks with preferential relocations to places visited in the past [4]. Similar notions can also be found in biological contexts, where organisms use stochastic resetting or switching between different phenotypic states to adapt to fluctuating environments [5–9]. In computer science, random walks with stochastic restarts turns out to be a useful strategy to optimize search algorithms in hard combinatorial problems [10–12].

The stochastic resetting mechanism has been shown to have rather rich and dramatic effects on the diffusion process [13–18], as well as on long-range jump processes such as Lévy flights [19]. While in the absence of the resetting, the diffusion in free space does not have a stationary state, a nonzero rate of resetting to a fixed position leads to a nonequilibrium stationary state (NESS) with non-Gaussian fluctuations, in the time $t \to \infty$ limit. Similarly, an extended system, such as a fluctuating interface, evolving under its own dynamics and is reset at a constant rate to its initial configuration, approaches at late times a NESS with a nontrivial interfacial height distribution [20]. Resetting-induced NESS has also been studied in other many-body systems, such as coagulation-diffusion processes [21].

While the mechanism by which the stochastic resetting leads to an eventual NESS has been well understood in the above studies, the approach to the NESS in such systems is yet to be addressed. The goal of this paper is to study this temporal relaxation to NESS in a wide variety of single-particle as well as many-body interacting systems, such as fluctuating interfaces. It is useful first to summarize our main results. We compute exactly the time-dependent probability distribution function (in presence of a resetting rate r) $P_r(x,t)$, where x may represent the position of a single particle undergoing a stochastic motion with resetting to the origin, or it may represent the height of a fluctuating interface at a fixed point in space with resetting to the initial condition. As $t \to \infty$, the system reaches the NESS characterized by $P_r(x,\infty)$. In systems without the $x \to -x$ symmetry, our solution at finite t shows that as time progresses, the NESS gets established in an inner core region $[-\xi_-(t),\xi_+(t)]$ around the point where the system is reset (which we take to be the origin O); outside this core regime, the system is still transient (see Fig. 1).

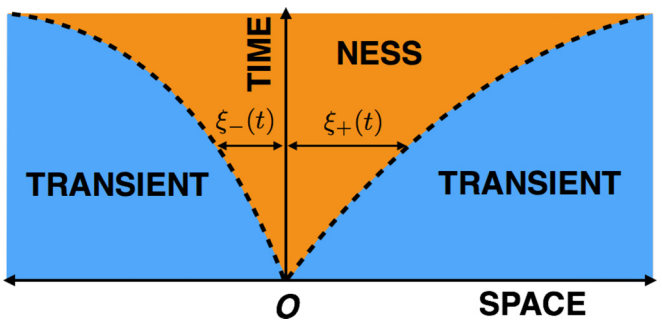

FIG. 1. (Color online) NESS gets established in a core region around the resetting center O whose right and left frontiers $\xi_\pm(t)$ grow with time. Outside the core region, the system is transient.

The frontiers $\xi_\pm(t)$, separating the inner NESS regime from the outer transient regime, typically grow with time as power laws, thus establishing NESS on larger and larger length scales. This phenomenon is conveniently captured by probing the probability density function (PDF) on the scale $x \sim \xi_\pm(t)$, where it has the large deviation form

$$P_r(x,t) \sim \exp\left[-t\, I\left(\frac{x}{\xi_\pm(t)}\right)\right], \tag{1}$$

where positive and negative fluctuations are scaled differently and $I(y)$ represents the large deviation function (LDF). For systems with $x \to -x$ symmetry, there is only a single length scale $\xi_+(t) = \xi_-(t) \equiv \xi(t)$ and $I(y)$ is symmetric. The LDF $I(y)$ characterizes the spatial dependence of the temporal relaxation. At different points x, the system relaxes with a different x-dependent rate. Alternatively, at a fixed point x, the system undergoes a dynamical transition from a transient to the stationary state at a characteristic time $t^*(x)$ such that $\xi_\pm(t^*) = x$ (for positive and negative x respectively). We compute $\xi_\pm(t)$ and $I(y)$ explicitly for several systems. We show that $\xi_\pm(t) \sim t^{1/\nu_\pm}$ typically grow algebraically at late times with a pair of new exponents. For the underlying stochastic process without resetting, the typical time-dependent length scale also grows algebraically $\sim t^{1/z}$ where z is the dynamical exponent, e.g., $z = 2$ for simple diffusion. In the presence of resetting, we show that $\nu_\pm$ are generically smaller than z. Furthermore, we show that the rate function $I(y)$ exhibits a universal feature: it has a pair of singular points at $y = y^*_+$ and $y = -y^*_-$, corresponding to the frontiers of the core region, signaling a dynamical phase transition. As discussed later, physically, this LDF $I(y)$ and its singularity provides a sharp spatiotemporal separation between typical and atypical trajectories of the underlying stochastic process with resetting. It turns out that, generically, the second derivative $I''(y)$ is discontinuous at this pair of singular points.

II. DIFFUSION OF A SINGLE PARTICLE

We begin with the simple example of a single particle diffusing in one dimension (generalization to higher dimensions is straightforward) whose position is stochastically reset to a fixed position (which is taken to be the origin without loss of generality) with a constant rate r. Let $P_r(x,t)$ be the probability density function (PDF) of the position x of the particle at time t. There arise two situations: one in which no resetting events occur during the observation time t (the probability of which being e^{-rt}) so that the particle moves from the origin to x as a free diffusion, and another in which the last resetting event before t occurs at time $t-\tau$ (and no resetting occurs in the remaining time τ; the PDF of which being $re^{-r\tau}$) so that the particle moves as a free diffusion in the final stretch of the time τ. Therefore, taking into account both situations (and integrating over τ), one gets [17]

$$P_r(x,t) = e^{-rt} P_0(x,t) + \int_0^t d\tau\, re^{-r\tau} P_0(x,\tau), \tag{2}$$

where $P_0(x,t) = \exp[-x^2/(4Dt)]/\sqrt{4\pi Dt}$ is the propagator for the particle to diffuse freely from the origin to the position x in time t in the absence of the resetting. The NESS is obtained by taking the $t \to \infty$ limit in Eq. (2), which yields [13]

$$P_r(x, t\to\infty) = \int_0^\infty d\tau re^{-r\tau} P_0(x,\tau) = \frac{\alpha}{2}\exp(-\alpha|x|), \tag{3}$$

where $\alpha = \sqrt{r/D}$. To analyze (2) for finite t, it is convenient to reexpress it using a change of variable $\tau = wt$, yielding

$$P_r(x,t) = \frac{e^{-t\Phi(1,x/t)}}{\sqrt{4\pi Dt}} + \frac{r\sqrt{t}}{\sqrt{4\pi D}}\int_0^1 \frac{dw}{\sqrt{w}}\, e^{-t\Phi(w,x/t)}, \tag{4a}$$

where

$$\Phi(w,y) = rw + \frac{y^2}{4Dw}. \tag{4b}$$

For large t and fixed $y = x/t$, the integral in the second term can be estimated by the saddle-point method. The function $\Phi(w,y)$ evidently has a single minimum with respect to w at $w^* = |y|/\sqrt{4Dr}$, obtained by setting $\partial_w \Phi(w,y)|_{w=w^*} = 0$. If $w^* < 1$, the saddle point occurs within the integration limits $w \in [0,1]$ and one gets, from Eq. (2) $P_r(x,t) \sim e^{-t\,\Phi(w^*,x/t)}$ for large t, where $\Phi(w^*,y) = \alpha\,|y|$. In contrast, for $w^* > 1$, the function $\Phi(w,y)$ has its lowest value in $w \in [0,1]$ at $w = 1$. Hence the integrand in the second term is dominated by the regime at $w = 1$ (and is of the same order as the first term). Physically, this corresponds to trajectories, which have undergone zero (or almost zero) resettings up to time t. One then gets $P_r(x,t) \sim e^{-t\,\Phi(1,x/t)}$, with $\Phi(1,y) = r + y^2/(4D)$. Summarizing, we obtain

$$P_r(x,t) \sim e^{-tI(x/t)}, \tag{5a}$$

where the LDF

$$I(y) = \begin{cases} \alpha\,|y| & \text{for } |y| < y^*, \\ r + \frac{y^2}{4D} & \text{for } |y| > y^*, \end{cases} \tag{5b}$$

with $y^* = \sqrt{4Dr}$.

Comparing Eq. (5a) with Eq. (1) shows that the growing length scale $\xi(t) \sim t$, much larger than the typical diffusion length scale $\sim \sqrt{t}$. The linearity of the LDF for $|y| < y^*$ implies that for any large but finite t there is an interior spatial region $-y^*t < x < y^*t$, where NESS has been achieved, as $P_r(x,t) \sim \exp(-\alpha|x|)$ becomes independent of t, in agreement with Eq. (3). However, there is still an exterior region $|x| > y^*t$ that has not been relaxed to the NESS yet. The boundaries between the two regions move at a constant speed y^*. From Eq. (5b), it is easy to check that while $I(y)$ and its first derivative are both continuous at $y = \pm y^*$, its second derivative has a discontinuity at $y = \pm y^*$. Therefore, the LDF has a second-order discontinuity at the points $\pm y^*$. Figure 2 shows very good agreement between the above large deviation form of the PDF and numerical simulations. The above analysis can be easily generalized to higher-dimensional diffusion as well as to other stochastic processes such as the fractional Brownian motion (see Appendix).

What is the physical significance of this phase transition? The probability density $P_r(x,t)$ can also be interpreted as the density at time t of a swarm of independent Brownian motions, each subjected to stochastic resetting with rate r, all starting from the origin at $t = 0$. Our calculation shows that at time t the density for $|x| < y^*t$ becomes stationary, while it is still time dependent for $|x| > y^*t$. From the analysis above, it is

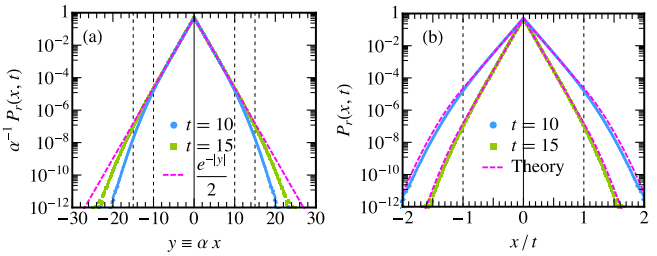

FIG. 2. (Color online) PDFs of the position of a particle diffusing in one dimension with a diffusion constant $D = 1/2$, whose position is stochastically reset to the origin at a constant rate $r = 1/2$. (a) The points are simulation data for the PDFs at $t = 10$ (blue circles) and $t = 15$ (green squares). The (magenta) dashed line is the infinite time NESS given in Eq. (3). The vertical dashed lines mark the positions $\pm y^* t$. (b) Same data as in (a) compared with large deviation result [Eq. (5)] of the PDF (normalized numerically), denoted by the (magenta) dashed lines. The dashed vertical lines at $y = \pm 1$ mark the y^* at which the LDF has a second order discontinuity.

clear that, for $|x| > y^* t$, the density is typically of the form $\sim e^{-r t} P_0(x,t)$ in Eq. (2), i.e., it corresponds to particles that have undergone almost no resetting up to time t. This is of course a very rare event and these particles in the outer region thus have very atypical trajectories. In contrast, the particles in the inner core region correspond to typical trajectories that have undergone a large number of resettings, leading to a stationary behavior in this regime. The LDF $I(y)$ in Eq. (5a) probes precisely the separation between these two regions, i.e., between the typical and the atypical trajectories. The singularity in the LDF signifies a sharp separation between these two types of particles. In any typical application of resetting, for instance, in the optimization of search algorithms, we would ideally like to keep, at any given finite time t, only the typical trajectories and not the atypical ones, since the latter ones are not affected by the resetting at all. The LDF $I(y)$ and its associated singularity, which sharply separates the two types of trajectories, thus provides a very useful and practical way to select the typical ones at any given time t. Even though we discuss it here in the context of a single-particle diffusion, it turns out that this picture is quite generic and holds for arbitrary stochastic processes undergoing resetting and even for spatially extended systems, such as fluctuating interfaces that we discuss next.

III. FLUCTUATING (1 + 1)-DIMENSIONAL INTERFACES

We next look at the effect of resetting on extended correlated objects such as a fluctuating interface growing with time over a linear substrate of size L. The interface is characterized by its height field $H(x,t)$, which typically evolves via a stochastic dynamics [22–24]. The height fluctuation is measured by the relative height field, $h(x,t) = H(x,t) - \overline{H(x,t)}$, where $\overline{H(x,t)} = L^{-1} \int_0^L dx\, H(x,t)$ is the spatially averaged height. The roughness of the interface is usually measured by the interface width $W(L,t)$ defined as $W^2(L,t) = \frac{1}{L} \int_0^L dx\, \langle h^2(x,t) \rangle$. For a large class of interfaces, $W(L,t)$ increases with time as $W(L,t) \sim t^\beta$ for $0 \ll t \ll L^z$, before saturating to a time-independent value $W_{\rm sat} \sim L^\alpha$ for $t \gg L^z$. The scaling exponents α, β, and z are known as the roughness exponent, growth exponent and dynamic exponent respectively, and are related by the scaling relation $z = \alpha/\beta$, leaving only two independent exponents [22]. Moreover, in the growing regime $0 \ll t \ll L^z$, the full height distribution $P_0(h,t)$ has the generic scaling form [22–24]

$$P_0(h,t) \approx (\Gamma t)^{-\beta} g[(\Gamma t)^{-\beta} h], \tag{6}$$

where the scaling function $g(x)$ is identical for all models belonging to the same universality class while Γ^{-1} is a model-dependent microscopic time scale. For example, for simple linear stochastic interface models belonging to the Edwards-Wilkinson (EW) universality class (where $\beta = 1/4$ and $z = 2$), the height distribution at all times is simply Gaussian [25] with $g(x) \propto \exp[-x^2]$. Another widely studied class of growing interfaces in $(1 + 1)$ dimensions belong to the Kardar-Parisi-Zhang (KPZ) universality class [22–24,26]. In this case one has $\beta = 1/3$ and $z = 3/2$ while the scaling function $g(x)$, for a flat initial condition $H(x,t = 0) = 0$, is related to the Tracy-Widom distribution [27] associated to the Gaussian Orthogonal Ensemble (GOE) of random matrices [28], $f_1(\chi)$, which describes the fluctuations of the largest eigenvalue of GOE matrices. One has indeed $g(x) = f_1(x + \langle \chi \rangle)$ where $\langle \chi \rangle = \int_{-\infty}^{\infty} d\chi f_1(\chi)$. While the full form of $f_1(\chi)$ is rather nontrivial, the tails have simpler non-Gaussian forms: $f_1(\chi) \sim \exp(-|\chi|^3/24)$ as $\chi \to -\infty$ and $f_1(\chi) \sim \exp(-2\chi^{3/2}/3)$ as $\chi \to \infty$.

Let us now consider the height field of such a generic $(1 + 1)$-dimensional interface evolving under its own dynamics and subject it to resetting to its initial height profile at constant rate r. Following our discussion prior to Eq. (2), one can relate the height distribution $P_r(h,t)$ in the presence of resetting to that of $P_0(h,t)$ without resetting via the same Eq. (2), with x replaced by h. Using the scaling form for $P_0(h,t)$ in Eq. (6) and making the change of variable $\tau = wt$, Eq. (2) reduces to

$$P_r(h,t) \approx (\Gamma t)^{-\beta} e^{-rt} g[(\Gamma t)^{-\beta} h] + rt(\Gamma t)^{-\beta} \int_0^1 dw\, w^{-\beta} e^{-rtw} g[(\Gamma t)^{-\beta} h w^{-\beta}]. \tag{7}$$

As before, $P_r(h,t)$ approaches a stationary distribution as $t \to \infty$ for any $r > 0$ [20]

$$P_r(h, t \to \infty) \approx (\Gamma/r)^{-\beta} G_\beta[(\Gamma/r)^{-\beta} h], \tag{8a}$$

where the scaling function is given by

$$G_\beta(x) = \int_0^\infty dy\, y^{-\beta} e^{-y} g(x y^{-\beta}). \tag{8b}$$

Now to investigate the approach to the NESS, we consider the generic case when $g(x) \sim \exp(-a_\pm |x|^{\gamma_\pm})$ as $x \to \pm\infty$. For example, for the KPZ with flat initial condition, $\gamma_+ = 3/2$, $a_+ = 2/3$ and $\gamma_- = 3$, $a_- = 1/24$. Substituting these generic tails of $g(x)$ in Eq. (A7) we obtain that the large deviation form

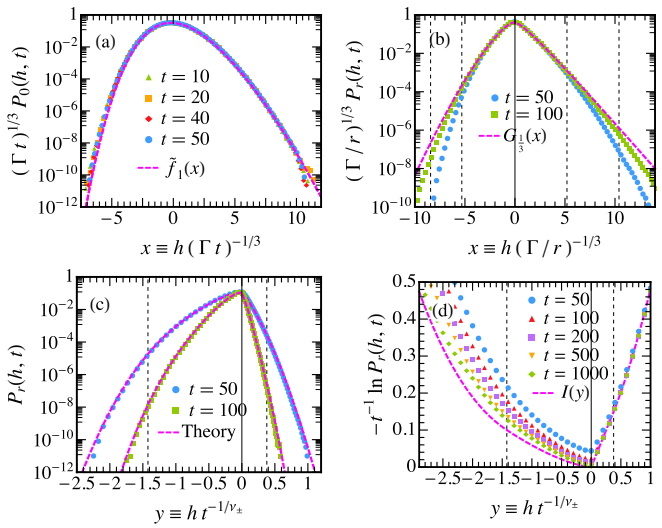

FIG. 3. (Color online) (a) The PDFs of the relative heights of a periodic interface of size $L = 2^{15}$ at various times, generated from a TASEP (shown by points) are collapsed by choosing $\Gamma = 2.4$ to the TW GOE PDF with zero mean, shown by the (magenta) dashed line. (b) The points are simulation data for the PDF of the relative heights at $t = 50$ (blue circles) and $t = 100$ (green squares), with resetting with rate $r = 0.05$. The (magenta) dashed line is the infinite time NESS given in Eq. (A8). The vertical dashed lines mark the positions $x^*_\pm = \pm y^*_\pm t^{1/\nu_\pm}$. (c) Same data as in (b) compared with Eq. (A7) denoted by the (magenta) dashed lines. The vertical dashed lines mark the positions $\pm y^*_\pm$. (d) The LDFs computed numerically from (A7) for various t are compared with (A10b).

of $P_r(h,t)$ (see Appendix)

$$P_r(h,t) \sim e^{-t\, I(h\, t^{-1/\nu_\pm})}, \tag{9a}$$

where the LDF is given by

$$I(y) = \begin{cases} \frac{r\,|y|^{\nu_\pm}}{\beta \nu_\pm (y^*_\pm)^{\nu_\pm}} & \text{for } |y| < y^*_\pm, \\ r + b_\pm |y|^{\gamma_\pm} & \text{for } |y| > y^*_\pm. \end{cases} \tag{9b}$$

The exponents $\nu_\pm = \gamma_\pm/(1+\beta\gamma_\pm)$ and the boundaries $y^*_\pm$ as well as the constants $b_\pm$ can be explicitly computed (see Appendix). The signs $\pm$ are chosen for $y > 0$ and $y < 0$ respectively. Comparing Eq. (A10a) and Eq. (1), we see that the growing scale, separating the inner NESS regime from the outer transient regime in the height space, $\xi_\pm(t) \sim t^{1/\nu_\pm}$ is asymmetric (different respectively for positive and negative height fluctuations). The height fluctuations in the intermediate range $-y^*_- t^{1/\nu_-} < h < y^*_+ t^{1/\nu_+}$ reaches NESS. Moreover, $I(y)$ again has a second order discontinuity at the two singular points $y^*_\pm$.

To perform simulations, we consider an interface model generated from the well known totally asymmetric simple exclusion process (TASEP) [29] on a ring. This interface model is known to belong to the KPZ class [22,24]. Figure 3(a) shows that the scaled PDF for various times in the growing regime ($1 \ll t \ll L^z$) can be collapsed by choosing a unique value of Γ (same for all t), to the TW GOE PDF with the mean shifted to zero. We use this value of Γ subsequently. We next simulate the dynamics of the interface in presence of resetting (with rate r) to the flat initial condition. It is evident from Fig. 3(b) that at long times the central part $|h| \ll t^{1/\nu_\pm}$ of the distribution of the relative heights reaches the NESS given by Eq. (A8). Figure 3(c) shows very good agreement between the simulation and the theoretical results obtained from numerical integration of Eq. (A7). In Fig. 3(d) we plot the LDFs computed numerically from (A7) for various t, which converges to (A10b) as time increases.

IV. DISCUSSION

In summary, we have studied analytically the approach to the stationary state of several systems subjected to resetting to the initial condition at a constant rate. We have shown that the relaxation mechanism in these systems is highly unusual. In typical systems approaching to their stationary states, the late time relaxation is governed by a single time scale independent of space. In systems with resetting studied here, the late time relaxation is space dependent and is characterized by the LDF $I[x/\xi(t)]$ defined in Eq. (1). The growing length (or height) scale around the resetting center behaves at late times as $\xi(t) \sim t^{1/\nu}$ where $\nu < z$ is a new exponent typically smaller than the dynamical exponent z of the process without resetting. For a system without the $x \to -x$ symmetry, such as in the KPZ equation, there are actually a pair of asymmetric length scales $\xi_\pm(t) \sim t^{1/\nu_\pm}$ where $\nu_\pm < z$. We have computed this LDF $I(y)$ explicitly in several examples and found that it exhibits a universal feature: it has a a pair of singular points where the second derivative is discontinuous. The singularities in $I(y)$ provide a sharp separation between typical and atypical trajectories and thus can be useful in various applications, such as search optimization using resetting, in detecting and getting rid of the undesirable atypical trajectories (that have not undergone resetting) at any finite time t. The important point is the presence of these singularities providing a sharp separation—the actual order of the singularities is of less relevance. We conclude by noting that singularities in the LDFs have also been found recently in several different contexts and there is a growing interest in understanding the significance of these singularities [30–36]. In this paper we have provided a clear physical meaning of these singularities that act like separatrices between typical and atypical trajectories.

ACKNOWLEDGMENTS

We acknowledge support of the Indo-French Centre for the Promotion of Advanced Research under Project No. 4604-3.

APPENDIX

In this Appendix, we give some details of the calculations described in the main text.

1. Fractional Brownian motion

The analysis of $P_r(x,t)$ carried out in the main text above for the simple Brownian motion can be easily generalized to the fractional Brownian motion (fBM), which represents a Gaussian process with zero mean and two-time correlator, $\langle x(t_1)x(t_2)\rangle = t_1^{2H} + t_2^{2H} - |t_1 - t_2|^{2H}$, where $0 < H < 1$ represent the Hurst index. Clearly $H = 1/2$ corresponds to the simple Brownian motion. For simplicity we discuss

the one-dimensional case, though generalization to higher dimensions is straightforward. The propagator for the fBM in one dimension, starting initially at the origin, again has the simple Gaussian form

$$P_0(x,t) = \frac{1}{\sqrt{4\pi\, D t^{2H}}}\, \exp\left[-\frac{x^2}{4\, D\, t^{2H}}\right]. \tag{A1}$$

We then subject the particle undergoing fBM to resetting at the origin with a constant rate r. Then, the propagator $P_r(x,t)$ in presence of the resetting satisfies the generic relation given by Eq. (2). Substituting the bare propagator $P_0(x,t)$ from Eq. (A1) in Eq. (2), we can then carry out the same analysis as the $H = 1/2$ case in the main manuscript. As in the case of $H = 1/2$, it turns out that for general $0 < H < 1$, the growing length scale $\xi(t) \sim t^{H+1/2}$, much larger than the typical spread $\sim t^H$ for large t. In the scaling limit $x \to \infty, t \to \infty$ with $x/t^{H+1/2}$ fixed, we obtain, using the saddle-point method (discussed already for $H = 1/2$ in the main manuscript)

$$P_r(x,t) \sim e^{-t\, I\left(x/t^{H+1/2}\right)}, \tag{A2a}$$

where the large deviation function (LDF) is

$$I(y) = \begin{cases} \alpha_H\, |y|^{\frac{1}{H+1/2}} & \text{for } |y| < y^*, \\ r + \frac{y^2}{4D} & \text{for } |y| > y^*, \end{cases}$$

$$\text{with} \quad \alpha_H = r\left(1+\frac{1}{2H}\right)\left(\frac{H}{2Dr}\right)^{\frac{1}{2H+1}} \quad \text{and} \quad y^* = \sqrt{\frac{2Dr}{H}}. \tag{A2b}$$

It is easy to check that both the LDF and its first derivative are continuous across $\pm y^*$, while the second derivative has a discontinuity at $\pm y^*$. The NESS is realized in an interior region where $P_r(x,t) \sim \exp(-\alpha_H\, |x|^{\frac{1}{H+1/2}})$ becomes independent of time, with the boundaries between this NESS and the outer transient regime moving out with time as $|x^*| = y^* t^{H+1/2}$.

2. Case of the Kardar-Parisi-Zhang equation

A widely studied class of growing interfaces in $(1+1)$ dimensions belongs to the Kardar-Parisi-Zhang (KPZ) universality class [22–24]. Here the height field evolves via the nonlinear KPZ equation [26]

$$\frac{\partial H}{\partial t} = \nu \frac{\partial^2 H}{\partial x^2} + \frac{\lambda}{2}\left(\frac{\partial H}{\partial x}\right)^2 + \eta(x,t), \tag{A3}$$

where ν is the surface tension, λ represents the strength of the nonlinearity, and $\eta(x,t)$ is a Gaussian white noise with zero mean and correlations $\langle \eta(x,t)\eta(x',t')\rangle = 2D\delta(x-x')\delta(t-t')$. In absence of nonlinearity ($\lambda = 0$), the KPZ equation (A3) reduces to the EW equation.

The scaling exponents for the KPZ equation in one dimension are well known [22]: $\alpha = 1/2$, $\beta = 1/3$, and $z = 3/2$. In the KPZ case, the spatially averaged height $\overline{H(x,t)} = L^{-1}\int_0^L dx\, H(x,t)$ grows linearly with time with a nonzero velocity $v_\infty = (\lambda/2)L^{-1}\int_0^L \langle (\partial H/\partial x)^2\rangle\, dx$. In contrast, for the EW case, $\overline{H(x,t)} \sim \sqrt{t/L}$ for large t. In the growing regime $0 \ll t \ll L^z$ to which we focus below, the PDF $P_0(h,t)$, while trivially Gaussian for the EW case, is highly nontrivial in the KPZ case and has been a subject of intense investigations in recent times. It has been solved exactly for the KPZ equation only very recently [28]. It turns out to depend on the initial condition of the height profile [28].

For example, for a flat initial profile, the height $H(x,t)$ of the interface can be written as

$$H(x,t) = v_\infty\, t + (\Gamma t)^{1/3}\chi(x), \tag{A4}$$

where Γ is a constant that depends on the parameters of the interface model, and χ is a time-independent random variable distributed according to the so-called Tracy-Widom (TW) distribution $f_1(\chi)$, which characterizes the fluctuations of the largest eigenvalue of random matrices in the Gaussian orthogonal ensemble (GOE) [27]. While the full form of $f_1(\chi)$ is rather nontrivial—the tails have simpler non-Gaussian forms: $f_1(\chi) \sim \exp(-|\chi|^3/24)$ as $\chi \to -\infty$ and $f_1(\chi) \sim \exp(-2\chi^{3/2}/3)$ as $\chi \to \infty$. In terms of χ, we have

$$h(x,t) = (\Gamma t)^{1/3}[\chi(x) - \overline{\chi}], \tag{A5}$$

where $\overline{\chi} = L^{-1}\int_0^L \chi(x)\, dx$. The law of large number dictates that $\overline{\chi} \to \langle\chi\rangle$ in the limit $L \to \infty$, so that $\langle h\rangle = 0$. Therefore, in this case, in the scaling limit of $t \to \infty$, $h \to \infty$ while keeping $h/t^{1/3}$ fixed, the height fluctuation is distributed according to

$$P_0(h,t) \approx (\Gamma t)^{-1/3}\, \widetilde{f}_1[(\Gamma t)^{-1/3}h], \tag{A6}$$

where $\widetilde{f}_1(x) = f_1\big(x + \langle\chi\rangle\big)$. This is indeed of the form announced in Eq. (6) in the main text above with $\beta = 1/3$ and $g(x) = \widetilde{f}_1(x)$. Similarly, for the droplet initial configuration (curved geometry), the scaling function for the height distribution is the TW distribution corresponding to the Gaussian unitary ensemble (GUE).

3. Generic interfaces: Saddle-point calculation

Let us now analyze the height field of a generic $(1+1)$-dimensional interface evolving under its own dynamics and subject it to resetting to its initial height profile at constant rate r. In this case, the full height distribution $P_0(h,t)$, in the absence of resetting ($r = 0$), has the generic scaling form [22–24] given by Eq. (6). As shown in the main text, one can relate the height distribution $P_r(h,t)$ in the presence of resetting to that of $P_0(h,t)$ without resetting via the Eq. (2) with x replaced by h. Using the scaling form for $P_0(h,t)$ in (6) and making the change of variable $\tau = wt$, it reduces to

$$P_r(h,t) \approx (\Gamma t)^{-\beta} e^{-rt}\, g[(\Gamma t)^{-\beta}h] + rt(\Gamma t)^{-\beta}\int_0^1 dw\, w^{-\beta} e^{-rtw}\, g[(\Gamma t)^{-\beta}hw^{-\beta}]. \tag{A7}$$

In this case, as in the case of single-particle diffusion, $P_r(h,t)$ approaches a stationary distribution as $t \to \infty$ for any $r > 0$, given by [20]

$$P_r(h, t\to\infty) \approx (\Gamma/r)^{-\beta} G_\beta[(\Gamma/r)^{-\beta}h], \tag{A8a}$$

where the scaling function is given by

$$G_\beta(x) = \int_0^\infty dy\, y^{-\beta} e^{-y}\, g(xy^{-\beta}). \tag{A8b}$$

Now to investigate the approach to the NESS, we consider the generic case when $g(x) \sim \exp(-a_\pm |x|^{\gamma_\pm})$ as $x \to \pm\infty$. For example, for the KPZ with flat initial condition, $\gamma_+ = 3/2$, $a_+ = 2/3$, and $\gamma_- = 3$, $a_- = 1/24$. Substituting these generic tails of $g(x)$ in Eq. (A7) we obtain

$$P_r(h,t) \sim (\Gamma t)^{-\beta} e^{-t\Phi(1,ht^{-1/\nu_\pm})} + rt(\Gamma t)^{-\beta} \int_0^1 dw\, w^{-\beta} e^{-t\Phi(w,ht^{-1/\nu_\pm})}, \quad \text{(A9a)}$$

where $\nu_\pm = \gamma_\pm/(1+\beta\gamma_\pm)$ and

$$\Phi(w,y) = rw + \frac{b_\pm |y|^{\gamma_\pm}}{w^{\beta\gamma_\pm}} \quad \text{with} \quad b_\pm = \frac{a_\pm}{\Gamma^{\beta\gamma_\pm}}. \quad \text{(A9b)}$$

With respect to the variable w, the function $\Phi(w,y)$ has a unique minimum at $w^* = (|y|/y_\pm^*)^{\nu_\pm}$, where $y_\pm^* = (r/[\beta\gamma_\pm b_\pm])^{1/\gamma_\pm}$. As in the case of single-particle diffusion discussed after Eq. (4b), if $w^* < 1$, the most dominant contribution to Eq. (A9a) comes from the neighborhood of w^* so that $P_r(h,t) \sim e^{-t\Phi(w^*,ht^{-1/\nu_\pm})}$, whereas for $w^* > 1$, it is dominated by the boundary terms so that $P_r(h,t) \sim e^{-t\Phi(1,ht^{-1/\nu_\pm})}$. Therefore, the large deviation form of $P_r(h,t)$ is given by

$$P_r(h,t) \sim e^{-t\, I(ht^{-1/\nu_\pm})}, \quad \text{(A10a)}$$

where the LDF is given by

$$I(y) = \begin{cases} \frac{r|y|^{\nu_\pm}}{\beta\nu_\pm (y_\pm^*)^{\nu_\pm}} & \text{for} \quad |y| < y_\pm^*, \\ r + b_\pm |y|^{\gamma_\pm} & \text{for} \quad |y| > y_\pm^*, \end{cases} \quad \text{(A10b)}$$

where the $\pm$ signs are chosen for $y > 0$ and $y < 0$ respectively. This yields the expression given in Eq. (9b), together with the explicit expression for the boundaries $y_\pm^*$ and for the constants $b_\pm$ [see Eq. (A9b) and below]. Moreover, one can show that $I(y)$ in (A10b) has a second-order discontinuity at the two singular points $y_\pm^*$.

4. Generic second-order discontinuity in the large deviation function

We now consider a generic system described by a stochastic variable x (which may represent the position of a particle undergoing generic stochastic dynamics, or may represent the height of a fluctuating interface). Let $P_0(x,t)$ be the bare probability density function (PDF) of x at time t, starting at $x = 0$, in the absence of resetting. Let $P_r(x,t)$ denote the PDF of x at time t in the presence of resetting to the initial condition $x = 0$ at a constant rate r. The PDF $P_r(x,t)$ is related to the bare propagator $P_0(x,t)$ via the general relation in Eq. (2). In the limit $t \to \infty$, $P_r(x,t)$ in Eq. (2) approaches the stationary distribution

$$P_r(x, t\to\infty) = r \int_0^\infty d\tau\, e^{-r\tau}\, P_0(x,\tau), \quad \text{(A11)}$$

which is fully determined by the bare PDF $P_0(x,t)$.

In order to study the approach to the stationary state at late times, we need to analyze Eq. (2) for finite but large t. To proceed, it is convenient to make a change of variable $\tau = w\,t$ in the integral, which yields

$$P_r(x,t) = e^{-r\,t}\, P_0(x,t) + r\,t \int_0^1 dw\, e^{-t\,r\,w}\, P_0(x, w\,t). \quad \text{(A12)}$$

We are interested in the behavior of $P_r(x,t)$ for large x and large t. Hence, inside the integral we need to substitute the large x, large t behavior (with w fixed) of $P_0(x,w\,t)$. For generic self-affine systems where $x(t) \sim t^\beta$, the PDF $P_0(x,t)$ is expected to have a scaling form, for large x, large t, keeping x/t^β fixed

$$P_0(x,t) \approx \frac{1}{(\Gamma\, t)^\beta}\, g\left(\frac{x}{(\Gamma\, t)^\beta}\right), \quad \text{(A13)}$$

where $g(y)$ is the scaling function and Γ^{-1} is a model-dependent microscopic time scale, not important for our analysis, and henceforth set to unity without any loss of generality. Substituting the scaling form Eq. (A13) of $P_0(x,t)$ in Eq. (A12) gives

$$P_r(x,t) = t^{-\beta}\, e^{-r\,t}\, g\left(\frac{x}{t^\beta}\right) + r\, t^{1-\beta} \int_0^1 \frac{dw}{w^\beta}\, e^{-t\,r\,w}\, g\left(\frac{x}{(w\,t)^\beta}\right). \quad \text{(A14)}$$

Next, we anticipate that $P_r(x,t)$ will have a large deviation form [see Eq. (1)]

$$P_r(x,t) \sim \exp\left[-t\, I\left(\frac{x}{\xi(t)}\right)\right], \quad \text{(A15)}$$

where $I(y)$ is the rate function and $\xi(t)$ represents the growing length scale associated with atypically large fluctuations of x that are much bigger than the typical fluctuations $x \sim t^\beta$. Note that in some cases (such as for the fluctuating interfaces belonging to the KPZ universality class), the $x \to -x$ symmetry is broken. In such cases, the positive and negative large fluctuations of x occur at different length scales $\xi_\pm(t)$ and accordingly, $P_r(x,t) \sim \exp\{-t\, I(x/\xi_\pm(t))\}$ for positive and negative fluctuations respectively [see Eq. (1)]. In these systems, we then need to scale the positive and negative fluctuations differently. However, in a problem with $x \to -x$ symmetry, there is only a single scale $\xi(t)$ and the LDF $I(y)$ is symmetric. For simplicity, we restrict ourselves below only to the positive fluctuations, as the analysis of the negative fluctuations is similar.

In order to probe the behavior of $P_r(x,t)$ on the scale $x \sim \xi(t) \gg t^\beta$, we then need to substitute the tail behavior of $g(y)$ for large y in the integrand of the second term in Eq. (A14). Generically, $g(y) \sim \exp[-a\, y^\gamma]$ for large positive y, where a is an unimportant model-dependent constant. Substituting this tail behavior in the integrand in Eq. (A14) we get

$$P_r(x,t) \sim t^{-\beta} e^{-t\Phi[1,x/\xi(t)]} + r\, t^{1-\beta} \int_0^1 dw\, w^{-\beta} e^{-t\Phi[w,x/\xi(t)]}, \quad \text{(A16)}$$

where $\xi(t) = t^{\beta+1/\gamma} \gg t^\beta$ and

$$\Phi(w,y) = r\, w + \frac{a\, y^\gamma}{w^{\gamma\,\beta}}. \quad \text{(A17)}$$

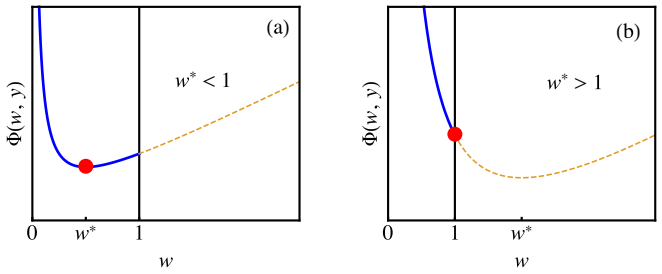

FIG. 4. (Color online) Schematic plot of the function $\Phi(w,y)$ as a function of w (but fixed y), which has a unique minimum at $w^*(y)$, determined from Eq. (A18) for the two cases (a) $w^* < 1$ and (b) $w^* > 1$. For the case (a), the integral in Eq. (A16) is dominated by the minimum w^*, whereas for the case (b) the integral is dominated by the upper limit $w = 1$ of the integral. The minimum values of $\Phi(w,y)$ in the interval $w \in [0,1]$ in both cases, are marked by the red circles.

Evidently $\Phi(w,y)$, as a function of w (but fixed y), has a unique minimum at $w^*(y)$, determined from

$$\partial_w \Phi(w,y)|_{w=w^*} = 0 \quad \text{where} \quad \partial_w \equiv \frac{\partial}{\partial w}. \tag{A18}$$

Actually the subsequent analysis will be very general and we do not need to use the specific form of $\Phi(w,y)$ —the only fact we will use is that $\Phi(w,y)$ has a unique minimum at $w^*(y)$, determined via the minimization in Eq. (A18).

For large t, the integral in Eq. (A16) is dominated by the minimum $w^*(y)$, as long as $w^*(y) < 1$, i.e., the saddle point lies within the limits of the integral $w \in [0,1]$, as shown in Fig. 4. For $w^*(y) > 1$, the integral is dominated by the upper limit $w = 1$ of the integral (see Fig. 4), which is of the same order as the first term. Thus, we have a critical point at $y = y^*$, which is determined from $w^*(y^*) = 1$. Thus, evaluating the integral in Eq. (A16) by the saddle-point method for large t gives the large deviation form given in Eq. (A15) where

$$I(y) = \begin{cases} \Phi(w^*(y),y) & \text{for} \quad y < y^*, \\ \Phi(1,y) & \text{for} \quad y > y^*. \end{cases} \tag{A19}$$

This is the generic mechanism of the dynamical transition—the rate function $I(y)$ changes its behavior at $y = y^*$. While the function $I(y)$ is evidently continuous at $y = y^*$, we show below that while its first derivative $I'(y)$ is also continuous at $y = y^*$, the second derivative $I''(y)$ is discontinuous, signaling a second-order dynamical transition.

Consider first a function of y of the form $H(y) = \Phi(u(y),y)$ where the first argument $u(y)$ depends implicitly on y. The derivatives of $H(y)$ can be easily determined by the chain rule. For example, the first derivative is given by

$$H'(y) = \frac{dH}{dy} = \partial_u \Phi(u,y)\, u'(y) + \partial_y \Phi(u,y). \tag{A20}$$

Similarly, the second derivative is given by

$$H''(y) = \partial_u^2 \Phi(u,y)\,[u'(y)]^2 + 2\,\partial_u \partial_y \Phi(u,y)\, u'(y) + \partial_u \Phi(u,y)\, u''(y) + \partial_y^2 \Phi(u,y). \tag{A21}$$

Now, let us first consider the case $y < y^*$ in Eq. (A19). To evaluate $I'(y)$, we substitute $u(y) = w^*(y)$ in Eq. (A20). Using the minimization condition in Eq. (A18), we obtain

$$I'(y) = \partial_y \Phi[w^*(y),y] \quad \text{for} \quad y < y^*. \tag{A22}$$

If now $y \to y^*$ from below, using $w^*(y^*) = 1$, we get

$$I'(y \to y^*) = \partial_y \Phi(1,y)|_{y=y^*}. \tag{A23}$$

For $y > y^*$ from above, we have $I(y) = \Phi(1,y)$ from Eq. (A19). Hence as $y \to y^*$ from above, $I'(y \to y^*) = \partial_y \Phi(1,y)|_{y=y^*}$. Comparing this with (A23), we see that $I'(y)$ is continuous at $y = y^*$.

We next consider the second derivative $I''(y)$ as $y \to y^*$ from below and above. Consider first the case $y < y^*$. Substituting $u(y) = w^*(y)$ in (A21) and using the minimization condition Eq. (A18), we get

$$I''(y) = \partial_{w^*}^2 \Phi(w^*,y)\,[(w^*)'(y)]^2 + 2\,\partial_{w^*}\partial_y \Phi(w^*,y)\,(w^*)'(y) + \partial_y^2 \Phi(w^*,y). \tag{A24}$$

Now, as $y \to y^*$ from below, $w^*(y) \to 1$ and we get

$$I''(y \to y^*) = \left\{\partial_{w^*}^2 \Phi(w^*,y)\,[(w^*)'(y)]^2 + 2\,\partial_{w^*}\partial_y \Phi(w^*,y)\,(w^*)'(y)\right\}\Big|_{w^*=1,y=y^*} + \partial_y^2 \Phi(1,y)\big|_{y=y^*}. \tag{A25}$$

In contrast, for $y > y^*$, $I(y) = \Phi(1,y)$ and hence $I''(y) = \partial_y^2 \Phi(1,y)$. Hence, as $y \to y^*$ from above, $I''(y \to y^*) = \partial_y^2 \Phi(1,y)|_{y=y^*}$. Comparing this with Eq. (A25), we see that generically the second derivative of the rate function is discontinuous across $y = y^*$ and the value of the discontinuity is given by

$$\lim_{\epsilon \to 0} [I''(y^* - \epsilon) - I''(y^* + \epsilon)] = \left\{\partial_{w^*}^2 \Phi(w^*,y)\,[(w^*)'(y)]^2 + 2\,\partial_{w^*}\partial_y \Phi(w^*,y)\,(w^*)'(y)\right\}\Big|_{w^*=1,y=y^*}. \tag{A26}$$

As an example, let us consider the case of diffusion with resetting (the first example in the main text). In this case, from Eq. (4b)

$$\Phi(w^*,y) = r\, w^* + \frac{y^2}{4\,D\,w^*}, \tag{A27}$$

where $w^*(y) = y/\sqrt{4Dr}$ (considering only the positive side). It is then straightforward to evaluate the discontinuity in Eq. (A26) and we get

$$\lim_{\epsilon \to 0} [I''(y^* - \epsilon) - I''(y^* + \epsilon)] = -\frac{1}{2D}. \tag{A28}$$

Similarly, one can obtain the value of the discontinuity in the second derivative for the other examples discussed in the main text.

[1] P. Turchin, *Quantitative Analysis of Movement* (Sinauer Associates Inc., Sunderland, Massachusetts, 1998).

[2] G. Vishwanathan, M. G. E. da Luz, E. P. Roposo, and H. E. Stanley, *The Physics of Foraging* (Cambridge University Press, Cambridge, 2011).

[3] O. Benichou, C. Loverdo, M. Moreau, and R. Voituriez, Rev. Mod. Phys. **83**, 81 (2011).

[4] D. Boyer and C. Solis-Salas, Phys. Rev. Lett. **112**, 240601 (2014).

[5] E. Kussell and S. Leibler, Science **309**, 2075 (2005).

[6] E. Kussell, R. Kishony, N. Q. Balaban, and S. Leibler, Genetics **169**, 1807 (2005).

[7] J. Reingruber and D. Holcman, Phys. Rev. Lett. **103**, 148102 (2009).

[8] P. Visco, R. J. Allen, S. N. Majumdar, and M. R. Evans, Biophys. J. **98**, 1099 (2010).

[9] J. Reingruber and D. Holcman, Phys. Rev. E **84**, 020901(R) (2011).

[10] L. Lovasz, in *Combinatronics* (Bolyai Society for Mathematical Studies, Budapest, 1996), Vol. 2, p. 1.

[11] A. Montanari and R. Zecchina, Phys. Rev. Lett. **88**, 178701 (2002).

[12] I. Konstas, V. Stathopoulos, and J. M. Jose, in *Proceedings of the 32nd International ACM SIGIR Conference* (ACM, New York, 2009), p. 195.

[13] M. R. Evans and S. N. Majumdar, Phys. Rev. Lett. **106**, 160601 (2011).

[14] M. R. Evans and S. N. Majumdar, J. Phys. A **44**, 435001 (2011).

[15] M. R. Evans, S. N. Majumdar, and K. Mallick, J. Phys. A **46**, 185001 (2013).

[16] J. Whitehouse, M. R. Evans, and S. N. Majumdar, Phys. Rev. E **87**, 022118 (2013).

[17] M. R. Evans and S. N. Majumdar, J. Phys. A **47**, 285001 (2014).

[18] A. Pal, Phys. Rev. E **91**, 012113 (2015).

[19] L. Kusmierz, S. N. Majumdar, S. Sabhapandit, and G. Schehr, Phys. Rev. Lett. **113**, 220602 (2014).

[20] S. Gupta, S. N. Majumdar, and G. Schehr, Phys. Rev. Lett. **112**, 220601 (2014).

[21] X. Durang, M. Henkel, and H. Park, J. Phys. A **47**, 045002 (2014).

[22] T. Halpin-Healy and Y.-C. Zhang, Phys. Rep. **254**, 215 (1995).

[23] A.-L. Barabási and H. E. Stanley, *Fractal Concepts in Surface Growth* (Cambridge University Press, Cambridge, 1995).

[24] J. Krug, Adv. Phys. **46**, 139 (1997).

[25] S. F. Edwards and D. R. Wilkinson, Proc. R. Soc. London A **381**, 17 (1982).

[26] M. Kardar, G. Parisi, and Y.-C. Zhang, Phys. Rev. Lett. **56**, 889 (1986).

[27] C. A. Tracy and H. Widom, Commun. Math. Phys. **159**, 151 (1994); **177**, 727 (1996).

[28] T. Sasamoto and H. Spohn, Phys. Rev. Lett. **104**, 230602 (2010); Nucl. Phys. B **834**, 523 (2010); P. Calabrese, P. Le Doussal, and A. Rosso, Europhys. Lett. **90**, 20002 (2010); V. Dotsenko, *ibid.* **90**, 20003 (2010); G. Amir, I. Corwin, and J. Quastel, Commun. Pure Appl. Math. **64**, 466 (2011); T. Halpin-Healy and Y. Lin, Phys. Rev. E **89**, 010103 (2014).

[29] T. M. Liggett, *Interacting Particle Systems* (Springer, Berlin, 2005).

[30] H. Touchette, Phys. Rep. **478**, 1 (2009).

[31] S. Sabhapandit, Europhys. Lett. **96**, 20005 (2011).

[32] N. Kumar, S. Ramaswamy, and A. K. Sood, Phys. Rev. Lett. **106**, 118001 (2011).

[33] S. Sabhapandit, Phys. Rev. E **85**, 021108 (2012).

[34] G. Bunin, Y. Kafri, and D. Podolsky, J. Stat. Phys. **152**, 112 (2013).

[35] A. Pal and S. Sabhapandit, Phys. Rev. E **87**, 022138 (2013).

[36] For a short review on singularities in the large deviation functions in the context of random matrix theory, see S. N. Majumdar and G. Schehr, J. Stat. Mech. (2014) P01012.